Electronic structure of random $Ag_{0.5}Pd_{0.5}$ and $Ag_{0.5}Au_{0.5}$ alloys

Z. W. Lu, S.-H. Wei, and Alex Zunger
Solar Energy Research Institute, Golden, Colorado 80401
(Received 20 November 1990; revised manuscript received 29 July 1991)

The electronic density of states and mixing enthalpies of random substitutional $A_{1-x}B_x$ alloys have often been described within the single-site coherent-potential approximation (SCPA). There one assumes that each atom interacts with a fictitious, highly symmetric average medium and that at a given composition x, all A atoms (and separately, all B atoms) are equivalent (i.e., have the same charges and atomic sizes). In reality, however, a random alloy manifests a distribution of different (generally, low-symmetry) local environments, whereby an atom surrounded locally mostly by like atoms can have different charge-transfer or structural relaxations than an atom surrounded mostly by unlike atoms. Such "environmental effects" (averaged out in the SCPA) were previously studied in terms of simple model Hamiltonians. We offer here an efficient method capable of describing such effects within first-principles self-consistent electronic-structure theory. This is accomplished through the use of the "special-quasirandom-structures" (SQS) concept [Zunger *et al.*, Phys. Rev. Lett. **65**, 353 (1990)], whereby the lattice sites of a periodic "supercell" are occupied by A's and B's in such a way that the structural correlation functions closely mimic those of a perfectly random infinite alloy. The self-consistent charge density, total and local density of states, and mixing enthalpies are then obtained by applying band theory (here, the linearized augmented-plane-wave method) to the SQS. Application to $Ag_{0.5}Pd_{0.5}$ and $Ag_{0.5}Au_{0.5}$ alloys clearly reveals environmental effects; that is, the charge distribution and local density of states of a given atomic site depend sensitively not only on the composition and occupation of the site but also on the distribution of atoms around it. This SQS approach provides a rather general framework for studying the electronic density of states of alloys.

I. INTRODUCTION

The electronic structure of substitutionally random alloys has been commonly discussed in terms of the electronic density of states (DOS) and its projection onto various atomic sites and angular momentum components[1-3] (local DOS, or LDOS). A central question surrounding such analyses is the extent to which the alloy environment modifies the DOS and LDOS of the constituent elemental solids. The basic issue surrounding such alloy-induced DOS variations can be defined as follows: Consider a *perfectly random* binary $A_{1-x}B_x$ alloy of composition x. At each x there are $N!/(xN)![(1-x)N]!$ ways ("configurations") of distributing the A and B atoms on a given lattice with N sites. Each configuration has its own "configurational DOS" and is distinguished from other configurations by the arrangement of atoms about each atomic site ("local environment"). In an arbitrary configuration, all A atoms (and, separately, all B atoms) can be crystallographically inequivalent. This geometrical inequivalence can drive then a concomitant electronic inequivalence in the properties of the various sites. For example, the net charge transfer Q_i on an atom (e.g., A at i) surrounded locally mostly by atoms of the *same* chemical type is likely to be smaller than that of the same atom surrounded locally mostly by atoms of the *opposite* type (i.e., B). Similarly, a large atom surrounded locally by smaller atoms can relax differently than the same large atom surrounded locally by atoms of equal sizes. Clearly, these "environmental effects" reflect the disparity between the properties of the mixed A and B species (electronegativities, atomic sizes, electron densities, and bandwidths) on the scale of alloy interactions, and they tend to vanish in alloys of nearly identical constituents (e.g., isotope mixtures to name an extreme example). Hence, even though the *occupation* statistics of sites in a random alloy may be (by assumption) perfectly random, the *physical properties* of each occupied site (net charges, configurational LDOS, local bonding geometries) need not take the (average) random values: these properties may indeed exhibit *correlations.* Since measurable alloy properties represent the ensemble average over all configurations, the central question surrounding the discussion of alloy effects on the DOS is the extent to which such "environmental effects" (at a fixed composition) survive alloy averaging.

Many theories of electronic structure of alloys provide no direct answer to this question, as environmental effects are averaged out at the outset. The "virtual-crystal approximation"[4] (VCA) averages over the properties of the A and B *atoms* (hence, all fluctuations are lost), whereas the (homogeneous) "site coherent-potential approximation"[5] (SCPA averages over the *environment* of each site, so that fluctuations in the properties of different A sites (and, separately, different B sites) are lost. More specifically, in performing a configurational average of a matrix representation P_{ij} of physical operators $\hat{P}$ (e.g., the scattering path operator) at particular atomic sites, the SCPA replaces the real atomic environment of the site by a *homogeneous* average medium of *identical,* "effective" scatters. Hence, in this single-site decoupling of the configurational average, only a single scatterer is

treated exactly while the rest are replaced by an effective medium (through which an electron travels unscattered). The scattering equation becomes analogous to that of a system with equivalent sites and the full symmetry of the pure A (or B) constitutent solids. While the SCPA constitutes the "best single-site model of an alloy",[1,5] it is not obvious if a single-site representation captures the essential physics for those physical properties that "see" the local environment. A few examples illustrate this doubt.

First, while the assumption (underlying the SCPA) of the equivalence of the properties of all A sites in a random configuration leads to a vanishing electrostatic Madelung (M) energy[6,7]

$$\langle E_M \rangle = \sum_{i \neq j} \frac{\langle Q_i Q_j \rangle}{R_{ij}} \equiv 0 , \tag{1}$$

a realistic model for the perfectly random alloy (permitting the magnitude of the point charges to depend on the occupation of nearest-neighbor sites, see below) yields a finite Madelung energy.[8,9] Assuming[6,7] $\langle E_M \rangle = 0$ then (significantly) overestimates "ordering energies." Hence, while the SCPA result $\langle E_M \rangle \equiv 0$ is *exact* within the mean-field model (that removes all geometrical information beyond single site), the model itself is unphysical in that it assumes that in a random configuration all A atoms have the same charge, irrespective of the chemical identity of the neighbors. Second, explicit calculations of the LDOS associated with a different local environment at a fixed global composition (e.g., a Pd atom coordinated by Pd_{12}, $Pd_{10}Ag_2$, Pd_6Ag_6, or Ag_{12} as first nearest neighbors in a random $Ag_{0.5}Pd_{0.5}$ alloy) exhibit distinct environmental effects.[10] Similar effects were discussed by Van der Rest, Gautier, and Brouers[11] and by Cyrot and Cyrot-Lackmann.[12] Third, simulation of the LDOS of large supercells with independently occupied sites[13–16] (leading naturally to a distribution of many different low-symmetry sites) often yields DOS features that are absent in the high-symmetry SCPA average. Fourth, while the assumption of equivalence of the A (or the B) sites leads to equal (average) $A-A$, $A-B$, and $B-B$ interatomic distances in a face-centered-cubic (fcc) alloy, extended x-ray-absorption fine-structure (EXAFS) experiments (e.g., in semiconductor[17–19] or metal[20,21] alloys) often exhibit unequal interatomic distances. We emphasize that the behaviors noted above are characteristic of nominally random alloys with no short- or long-range order. Extensions of the CPA formalism so that scattering from objects larger than a single site can be created more accurately[22–25] [e.g., molecular CPA,[22] next-neighbor CPA (Ref. 15)] have been attempted. While constant progress is being made along these directions,[26] the complexity of such models, however, has not been conducive so far to the use of first-principles electronic Hamiltonians that permit full (i.e., position-dependent) charge self-consistency while permitting general atomic relaxations.

In principle, the most straightforward approach to the evaluation of the electronic density of states of a $A_{1-x}B_x$ random alloy entails application of an electronic Hamiltonian to a "large" supercell whose $N \to \infty$ sites are occupied independently by A and B. Such a model would naturally exhibit (when $N \to \infty$) all possible local environments about the various atomic sites without resorting to a single-site decoupling. Applications of a Hamiltonian to describe the electronic structure of such a giant supercell would, in principle, yield an "exact" description of the DOS of the random alloy. In practice, such supercell calculations were limited to $N = O(10^3)$ atoms, e.g., the $\sim$1000-atom cell of $Pb_{1-x}Sr_xS$ used by Davis,[13] the $\sim$2000-atom model of $(GaAs_{1-x}Ge_{2x}$ used by Davis and Holloway,[14] the $\sim$2000-atom model of $Al_{1-x}Ga_xAs$ used by Hass, Davis, and Zunger,[16] and the earlier model calculations by Alben *et al.*[15] with 8000–10 000 atoms. By necessity, such model calculations are limited to highly simplified electronic Hamiltonians (e.g., subminimal basis-set tight-binding models) and neglect atomic relaxation. First-principles theories of electronic structure[27–29] are currently limited to $N \leq 50$ atoms/cell. For such small supercells, a "random" (coin-flip) occupation of the site by A and B atoms produces a structure that, as a whole, can deviate substantially[30,31] from randomness (a deviation measured by the amount that its many-body correlation functions fail to match those of the perfectly random network).

We have recently noted[30,31] that it is possible to occupy the N sites of a supercell by A and B atoms in such a way that its correlation functions approach those of a random network far closer than granted by the conventional method[13–16] of occupying randomly one site at the time. The basic concept can be appreciated as follows: In general, any lattice property P (total energy, DOS, volume) can be rigorously expanded[32] in a series of contributions p_f from "figures" f:

$$P(\sigma) = \sum_f \Pi_f(\sigma) p_f ,$$

where σ denotes the lattice configuration and $\{\Pi_f(\sigma)\}$ are the spin products for figure f in configuration σ. The "special quasirandom structure" (SQS) is constructed by selecting site occupation (in an N-atom unit cell) by A's and B's such that the quantities $\{\Pi_f(\mathrm{SQS})\}$ best match the *exact* configurational average $\langle \Pi_f \rangle$ in an infinite random alloy. For a small number of atoms $N \sim O(10)$ per cell, this can be accomplished only for a few "figures" f; we hence select the SQS so that the *first* few pair and many-body Π_f's match those of the exact random system. If two structures have the same $\{\Pi_f\}$ to all orders, they must be the same structure with the same P. Also if two different structures have the same Π_f up to a certain range, and p_f are zero beyond this range, then these two structures also have the same property P. This clarifies the source of error in the SQS: an error occurs when a physical property P requires for its description longer-range figures $\{f\}$ then the size used in constructing the SQS. Possible examples for such properties are the x-ray scattering factors [studied in Ref. 31(a)]. On the other hand, we find that properties such as the equilibrium molar volume,[9] total energy,[9] and LDOS,[31(b)] and bond lengths around an atom are influenced mostly by the "local environment" (e.g., up to $\sim$ the fourth fcc neighbor), so the SQS forms an adequate approximation. As the size of the SQS-N increases, more Π_f's can be matched to the

exact random values, so the predictions improve successively.

For the fcc $A_{0.5}B_{0.5}$ alloy, for example, the SQS-8_a consists of an eight-atom supercell best defined as an $A_1B_2A_3B_2$ superlattice along the [113] direction (i.e., one monolayer of A, followed by two monolayers of B, followed by three monolayers of A, and finally by two monolayers of B, all perpendicular to the [113] direction). Figure 1 depicts this structure. Note that swapping A and B yields the SQS-8_b superlattice $B_1A_2B_3A_2$. In what follows, we will study the electronic structure of the $Ag_{0.5}Pd_{0.5}$ and $Ag_{0.5}Au_{0.5}$ equiatomic alloys through the SQS concept, using the local-density functional formalism (LDA),[33,34] as implemented by the linearized augmented-plane-wave (LAPW) method.[35] A close representation of random alloys can be obtained by averaging the results of SQS-8_a and SQS-8_b.

There are three noteworthy properties of this approach. First, the SQS's naturally exhibit a *distribution* of (low-site symmetries) inequivalent A sites (and, separately, B sites). It hence provides the opportunity to assess environmental effects on the DOS, LDOS, and charge distribution. Figure 1 denotes the various atomic sites by superscripts that indicate the number of like neighbors in the first coordination shell. Note that in a perfectly random fcc alloy at $x=\frac{1}{2}$ the exact average number of atoms of opposite type to that at the origin is[31(a)] $6\pm\sqrt{3}$, $3\pm\sqrt{1.5}$, $12\pm\sqrt{6}$, $6\pm\sqrt{3}$, $12\pm\sqrt{6}$, and $4\pm\sqrt{2}$ for the first through sixth coordination shells, respectively. The SQS-8 yields[31(a)] 6 ± 1.8, 3 ± 0.5, 11.5 ± 1.4, 6.5 ± 0.5, 11 ± 1.4, and 4 ± 1.0, respectively, all within the exact fluctuation range. Note further that the average of the SQS-8_a and SQS-8_b contains all five $A_{4-n}B_n$ $(0\le n\le4)$ nearest-neighbor tetrahedra in the correct random probability ratios 1:4:6:4:1 for $x=\frac{1}{2}$.

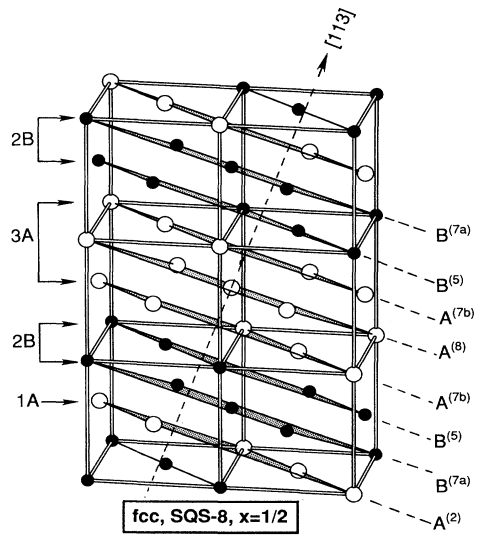

FIG. 1. Crystal structure of the binary $A_{0.5}B_{0.5}$ fcc SQS-8 at composition $x=\frac{1}{2}$. Lattice vectors and atomic coordinates are given in Eqs. (2) and (3), respectively. The shaded areas denote planes perpendicular to the [113] direction. Superscripts denote the number of like atoms in the first coordination shell around a given site. Open and solid circles denote A- and B-type atoms, respectively. SQS-8_a and SQS-8_b are distinguished by swapping A and B.

Second, since the SQS's are rather simple periodic structures with a small number of atoms per unit cell, their electronic properties (total energy, equilibrium lattice parameters, DOS, LDOS, and charge densities) can be efficiently calculated from first principles[27–29] with the same degree of sophistication with which ordinary simple crystals are currently treated.

Third, this SQS is indeed "special" in the sense that such a *single* eight-atom structure closely mimics the *configurational average* of the properties of far larger, randomly occupied supercells. The tests conducted to date to this effect were described elsewhere;[8,16,30,31,36] they are summarized briefly below.

(i) An $\sim$ 2300-atom configuration of the $Al_{0.5}Ga_{0.5}As$ alloy was generated[16] through random site-by-site occupation of the underlying zinc-blende lattice. This structure was then subjected to an electronic tight-binding Hamiltonian solved by the recursion method. This provided the spectral functions for various zinc-blende wave vectors. The same tight-binding Hamiltonian was separately applied to the SQS-8 model appropriate to such a pseudobinary alloy. The two calculations yield $\Gamma_{15v}-\Gamma_{1c}$, $\Gamma_{15v}-X_{1c}$, $\Gamma_{15v}-X_{3c}$, and $\Gamma_{15v}-L_{1c}$ band gaps (typically around $\sim$2 eV) which are within 0.02 eV or less from each other. The SQS calculation also reproduces closely the *distribution* of states, as measured by the second moment of the spectral functions at various wave vectors in the zinc-blende Brillouin zone. (In fact, for certain states, the SQS reproduces the moments obtained in the recursion calculations considerably better than CPA.)

(ii) For semiconductor alloys, a single total energy calculation on SQS-8 reproduces closely the mixing enthalpy of the random alloy calculated separately by summing over the contributions of pair interactions up to the sixth neighbor, as well as the first few three- and four-body terms.[30,31]

(iii) Minimization of the total elastic energy of $\sim$1000-atom supercells of random $Si_{0.5}Ge_{0.5}$ and averaging over a sufficient number of random configurations produces total elastic energies that are within 0.2 meV/atom of what a single, eight-atom SQS gives.[36]

(iv) The Madelung constant α_m for a single SQS-N of a fcc alloy are very close to the *exact* configurationally averaged value for an infinite fcc random alloy.[8] We find the Madelung constants $\alpha_M=0.588\,82$, $0.754\,45$, and $0.740\,31$ for SQS-4, SQS-8, and SQS-16, respectively, approaching the exact random alloy value ($\alpha_M=0.739\,52$) quite rapidly as a function of N. The SCPA result[26(d)] ($\alpha_M=0$) is very different.

This paper describes the first application of the SQS to metal alloys. Section II describes the basic physical properties of the Ag-Pd and Ag-Au systems which motivated our choice for them in the present study. Section III briefly describes the method used to perform the calculation, while Sec. IV describes our results for the alloy's enthalpies and equilibrium lattice constants (A), charge distribution (B), LDOS and their interpretation (C and

D), and total DOS (E). Section V summarizes the main conclusion: we find that the present approach gives a realistic alloy DOS, exhibits environmental effects lacking in the SCPA, and is easier to apply.

II. CHOICES OF ALLOY SYSTEMS

We have selected for this first application of the SQS concept to metal alloys two fcc systems: AgPd and AgAu. The AgPd system was chosen primarily because it appears to be very popular among practitioners of the SCPA: it has been previously treated by the Korringa-Kohn-Rostoker (KKR)-CPA [Refs. 1, 10, 21(c), and 37–45] method (both self-consistently[43] and non-self-consistently[39]), tight-binding CPA,[45] model Hamiltonian CPA,[44] and linear-muffin-tin-orbitals CPA.[21(c)] For AgAu, there was a previous non-self-consistent relativistic KKR-CPA calculation.[46] To develop an intuition on the anticipated properties of this alloy system and those for AgAu, we have collected in Table I (Refs. 47–51) some data on the relevant Pd, Ag, and Au free atoms [LDA (Refs. 50,51) calculated atomic s and d orbital energies and the phenomenological Pauling's electronegativities[47]] and the elemental solid metals (LAPW-calculated positions and widths of d bands, measured photoelectric work functions,[48] and equilibrium lattice parameters[49]). For the same purpose, Fig. 2 compares our LAPW calculated radial (total and valence) charge densities of the pertinent fcc elemental solids while Figs. 3 and 4 give their calculated total density of states.

TABLE I. Collection of various properties of the free atoms and elemental fcc solids of Pd, Ag, and Au. ε_d and ε_s are atomic orbital energies calculated semirelativistically within the LDA using the exchange-correlation function of Refs. 50 and 51. $\langle R_d \rangle$ is the expectation value of the atomic d orbital radii obtained with the same atomic calculations. $\varepsilon_d^\Gamma - \varepsilon_F$ is the LAPW calculated highest d band position in the solid at the Γ point, and W_d^Γ and W_d^X are the LAPW calculated d band widths (difference between the highest and lowest d band positions) at Γ and X, respectively. Φ, χ, and a are the photoelectric work function, the Pauling electronegativity, and room temperature lattice constants, respectively. The quantities displayed in this table are used in the text to discuss qualitative expectations on alloy behavior.

Quantity	Pd	Ag	Au
ε_d (atom,eV)	−4.31	−7.66	−7.12
ε_s (atom,eV)	−3.62	−4.72	−6.09
$\langle R_d \rangle$ (atom,Å)	0.841	0.751	0.857
$\varepsilon_d^\Gamma - \varepsilon_F$ (solid,eV)	−1.14	−3.82	−3.24
$-\Phi$ (eV)	−5.55±0.1[a]	−4.0±0.15[a]	−5.1±0.1[a]
χ	2.2[a]	1.9[b]	2.4[b]
W_d^Γ (solid, eV)	1.73	1.06	1.55
W_d^X (solid,eV)	6.04	3.74	5.48
a (solid,Å)	3.8898[c]	4.0862[c]	4.0783[c]

[a]Reference 48. Note that experimental photoelectric work functions include an unspecified surface contribution; hence, it can be used only to judge qualitatively the direction of charge transfer.
[b]Reference 47.
[c]Reference 49.

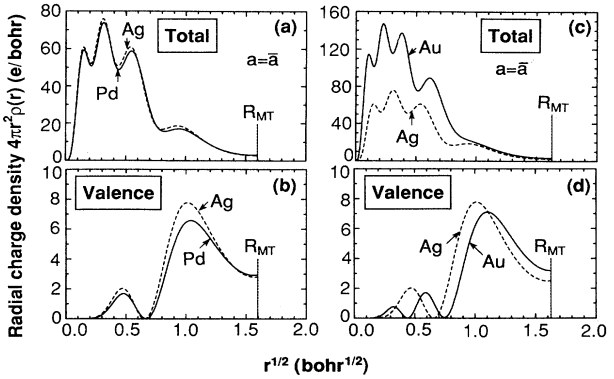

FIG. 2. LAPW calculated radial charge densities of the elemental fcc metals within the muffin-tin spheres of radius R_{MT}. (a) Ag and Pd total charge density, (b) Ag and Pd valence-only charge density, (c) Ag and Au total charge density, (d) Ag and Au valence-only charge density. To better resolve the structure shown, these functions are plotted vs $r^{1/2}$, not r. The plots for Ag and Au are done near the experimental lattice constant $a=4.080$ Å and $R_{MT}=2.65$ a.u. For Ag and Pd, we show results at the calculated *alloy* lattice constant $\bar{a}=3.928$ Å and $R_{MT}=2.55$ a.u.

Regarding Ag-Pd, the significant separation between the Pd and Ag d levels in the free atoms (Table I) and solids (Fig. 3) on the scale of the bandwidth in the condensed phases (Fig. 3) is suggestive of possible "split band behavior," where the states in the AgPd alloy retain to a large extent their characteristics of the pure phases. We hence expect significant environmental effects on the *density of states.* Furthermore, since Ag and Pd have different numbers of valence electrons (11 and 10, respectively) and Fermi surface DOS, environmental effects on the *charge transfer* may also be significant.

The situation regarding AgAu is different. There, the Au atomic s level is considerably deeper (due to relativistic contraction) than the outer Ag s level, suggesting a Ag→Au s charge transfer. Such an overall direction of charge transfer is also suggested by the sizable electronegativity difference[47] ($\chi_{Au}=2.4$ and $\chi_{Ag}=1.9$) and work function difference[48] ($\Phi_{Au}=5.1$ eV and $\Phi_{Ag}=4.0$ eV). On the other hand, the Au d level is slightly (0.5 eV in the free atoms, 0.75 eV in the elemental solids) *above* the Ag d level (also a relativistic effect), suggesting a possible *reversed* Au→Ag d electron charge transfer. Silver and gold differ significantly, not only in their propensities to transfer or accept charge but also in their valence charge density [Figs. 2(c) and 2(d)]. We hence expect significant environment effects on the *charge transfer.* On the other hand, the similarity of the d band energies and the significant overlap of the density of states of Ag and Au suggest a "common band" behavior and weaker environmental effects *on the DOS.*

III. METHOD OF CALCULATION

A. Determination of structural parameters

The fcc SQS-8 at $x=\frac{1}{2}$ has the monoclinic unit cell (space group[52] C_{2h}^1) with lattice vectors:

$$\mathbf{a}=(0.5,-0.5,0.0)a\ ,$$
$$\mathbf{b}=(1.0,0.5,-0.5)a\ , \quad (2)$$
$$\mathbf{c}=(1.0,1.0,2.0)a\ ,$$

where a is the lattice constant. The atomic positions (in Cartesian coordinates) take the general form

$$\tau_i=(x_i,x_i,z_i)a\ . \quad (3)$$

The ideal (unrelaxed) atomic positions for SQS-8_a (Fig. 1) in Cartesian coordinates are:

$$A^{(2)}=(0.5,0.5,1.0)a\ ,$$
$$A^{(7)}=(0.5,0.5,0.0)a;(-0.5,-0.5,0.0)a\ ,$$
$$A^{(8)}=(0.0,0.0,0.0)a\ , \quad (4)$$
$$B^{(5)}=(-0.5,-0.5,1.0)a;(0.5,0.5,-1.0)a\ ,$$
$$B^{(7)}=(0.0,0.0,1.0)a;(0.0,0.0,-1.0)a\ .$$

Here, the number in the superscript is the number of like atoms in the nearest-neighbor shell.

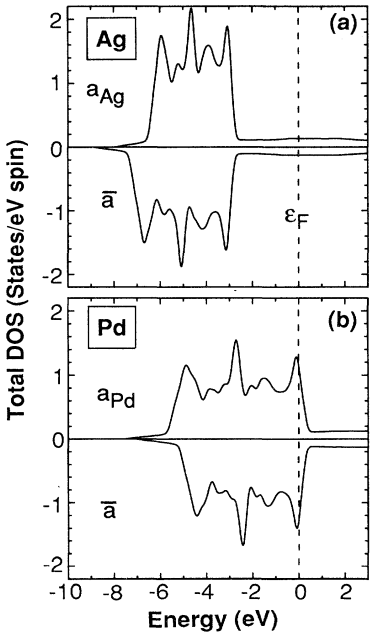

FIG. 3. Total density of states (in the whole space, not MT spheres) of the elemental fcc solids: (a) Ag near its experimental lattice constant $a_{Ag}=4.080$ Å and at the 50%-50% average (Ag-Pd) lattice constant $\bar{a}=3.928$ Å. (b) Pd at its calculated equilibrium lattice constant $a_{Pd}=3.848$ Å and at its 50%-50% average (Ag-Pd) lattice constant $\bar{a}=3.928$ Å. Note how compression (dilation) of Ag (Pd) broadens (narrows) the bandwidth and shifts the states to deeper (shallower) binding energies with respect to ε_F (dashed line, taken as zero energy).

B. Electronic Hamiltonian and its solution

The equilibrium values of the lattice constants are obtained by minimizing the total electron-plus-ion energy of the SQS. Cell-internal atomic relaxations are neglected. We calculate the electronic properties of the alloy in the local-density approximation[33,34] with the Ceperley-Alder[50] exchange-correlation functional as parametrized by Perdew and Zunger.[51] The LDA equations are solved by the LAPW method,[35] in which fully self-consistent solutions to the effective single-particle equations are found, without restricting the shape of the potential and charge density. Inside the muffin-tin (MT) spheres, the nonspherical charge density and potential are expanded in terms of lattice harmonics of angular momentum $l \leq 8$. A basis set of 50–55 LAPW's/atom are used (equivalent to kinetic energy cutoffs of 9.83 Ry for AgPd and 9.11 Ry for AgAu). During the self-consistency iterations, the Brillouin zone summation was done using 60 special **k** points[53] for the fcc constituents and 98 special **k** points for SQS, respectively. All calculations were carried out semirelativistically, except for fcc Ag and Au, which were also calculated fully relativistically. The muffin-tin radii of A and B atoms were chosen to be equal: in the AgPd alloy and its elemental solids $R_{MT}^{Ag}=R_{MT}^{Pd}=2.55$ a.u., while in the AgAu alloy and its elemental solids $R_{MT}^{Ag}=R_{MT}^{Au}=2.65$ a.u. The densities of states are calculated using the tetrahedron integration method.[54] The resulting DOS were then smoothed using a Gaussian function with a full width at half maximum of about 0.2 eV. The energy eigenvalues are evaluated at 195 and 117 **k** points in the irreducible Brillouin zones for the fcc constituents and the SQS-8 structure, respectively.

Our results for the electronic states in the elemental Ag, Pd, and Au fcc solids are summarized in Table II,[55–64] where they are compared with other band-structure calculations[55,56,58,61] and experiments.[62–64]

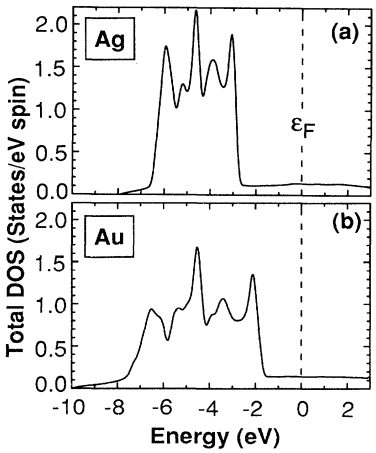

FIG. 4. Total density of states (in the whole space, not MT spheres) of (a) Ag and (b) Au at $a=4.080$ Å [close to the individual experimental lattice constants of Ag and Au, see Eq. (5)]. The zero of energy is at ε_F, denoted by vertical dashed line.

The calculated equilibrium lattice parameters of the pure solids are

$$a(\mathrm{Ag})=4.008\ \text{Å},\quad a(\mathrm{Au})=4.056\ \text{Å},\quad a(\mathrm{Pd})=3.848\ \text{Å} \tag{5}$$

compared with the room-temperature experimental data[49]

$$a(\mathrm{Ag})=4.086\ \text{Å},\quad a(\mathrm{Au})=4.078\ \text{Å},\quad a(\mathrm{Pd})=3.890\ \text{Å} \tag{6}$$

and the pseudopotential mixed-basis results of Takeuchi *et al.*[65]

$$a(\mathrm{Ag})=4.108\ \text{Å},\quad a(\mathrm{Au})=4.104\ \text{Å}\ . \tag{7}$$

IV. RESULTS

A. Mixing enthalpies and equilibrium lattice parameters

The mixing enthalpy ΔH of the $x=\frac{1}{2}$ random alloys were obtained by minimization of the SQS-8 total energy versus lattice constant. ΔH is the difference between the SQS total energy at a_{eq} and the total energies of the equivalent amounts of the solid constituents at their equilibrium lattice constants [Eqs. (5) and (6)]. Figure 5(a) shows such a calculation for $Ag_{0.5}Pd_{0.5}$, yielding

$$\Delta H(x=\tfrac{1}{2})=-38.3\ \text{meV/atom} \tag{8}$$

and

$$a_{\mathrm{eq}}=0.998\bar{a}\ ,$$

where $\bar{a}=3.928$ Å is the linear average of the calculated [Eq. (5)] lattice parameter of Ag and Pd. This can be compared with the experimental results

$$\Delta H(x=\tfrac{1}{2},\ T=1200\ \text{K})=-52.1\ \text{meV/atom (Ref. 66)} \tag{9}$$

and

$$a_{\mathrm{eq}}(T=295\ \text{K})\approx 1.007\bar{a}_0\ \text{(Ref. 67)}\ ,$$

where $\bar{a}_0$ is the linear average of the experimental lattice constants of Ag and Pd. The less negative value of the calculated ΔH is in part due to our neglect of the cell-internal relaxations. Note that $\Delta H<0$ for the random alloy implies a tendency toward short-range order in the al-

TABLE II. d band widths (W_d) and positions (ε_d) in fcc, Pd, Ag, and Au. Results have been listed in each case for the three high-symmetry **k** points Γ, L, and X. The s band position at the Γ point is also listed. The width is defined here as the energy difference between the highest and lowest d band eigenvalues at the *respective* **k** *point*. The *position* is defined as the highest d band eigenvalue. All energies are in mRy and are measured with respect to the Fermi energy. The last column gives the density of states $D(\varepsilon_F)$ (in states/eV spin) at the Fermi energy. SR and R denote "semirelativistic" and "relativistic," respectively.

			Γ		X		L		
	Metal	ε_s	ε_d	W_d	ε_d	W_d	ε_d	W_d	$D(\varepsilon_F)$
Present (SR)		−551	−84	127	25	444	1	413	1.193
LAPW[a]	Pd	−528	−90	133	34	434	5	400	1.283
Experiment[b]			−85	103			−7		
Present (SR)		−581	−281	78	−205	275	−221	257	0.135
Present (R)		−581	−276	96	−190	291	−211	268	0.135
LAPW[c]	Ag		−295	90	−209	273	−232	250	0.131
RAPW[d]			−349	85	−274	250	−292	218	0.127
Experiment[e]			−351	84			−291	219	
Present (SR)		−734	−238	114	−124	403	−148	398	0.143
Present (R)		−744	−229	177	−86	457	−128	434	0.149
LAPW[c]	Au		−233	175	−86	464	−130	435	0.142
RAPW[f]			−257	170	−121	431	−161	386	
Experiment[g]			−261	173					

[a]Reference 55, fully relativistic LAPW calculation, using Hedin-Lundqvist exchange-correlation (Ref. 57) potential.
[b]Reference 62.
[c]Reference 56, fully relativistic LAPW calculation, using the Hedin-Lundqvist exchange-correlation potential.
[d]Reference 58, using non-self-consistent relativistic augmented-plane-wave method (RAPW, Ref. 59) with the $X\alpha$ ($\alpha=1$, Ref. 60) exchange-correlation potential.
[e]Reference 63.
[f]Reference 61, using non- self-consistent RAPW method with the $X\alpha$ ($\alpha=1$) exchange-correlation potential.
[g]Reference 64.

loy and possible long-range order at low temperature. This result conflicts with the simple expectation based on the tight-binding model[68] that binary alloys of all late transition metals should phase separate rather than order. To examine this issue more closely, we have calculated the formation enthalpies of *ordered* AgPd in the $L1_0$ (CuAu-I), $L1_1$ (CuPt), and $B2$ (CsCl) structures (Fig. 5), finding that $\Delta H(L1_1) = -60.4$ meV/atom; that is, this structure is stable both with respect to phase separation ($\Delta H < 0$, as also noticed by Takizawa and Terakura[69]) and disordering at $T=0$ [i.e., $\Delta H(L1_1) < \Delta H(\mathrm{SQS})$]. The $B2$ structure is unstable with respect to phase separation [it has $\Delta H(B2) = +19.7$ meV/atom and, therefore, is outside the range in Fig. 5]. Low-temperature studies of possible $L1_1$ ordered phases in the Ag-Pd system are lacking (the existing phase diagram[70] is limited to rather high temperatures, $T \gtrsim 1200$ K, exhibiting continuous fcc solid solutions). Diffused scattering experiments on the disordered alloy could potentially indicate such ordering tendencies.

For the AgAu random alloy, we find the mixing enthalpy and lattice constant

$$\Delta H(x=\tfrac{1}{2}) = -44.7 \text{ meV/atom}, \qquad a_{\mathrm{eq}} = 0.998\bar{a}, \tag{10}$$

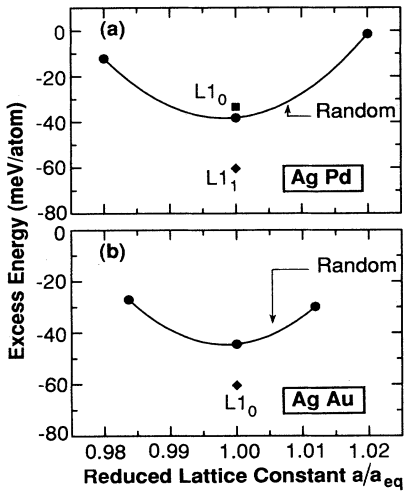

FIG. 5. Calculated excess energy $\Delta E(a)$ vs lattice constant a for the random alloys (modeled by the energy of SQS-8 and shown as solid circles and solid lines) and some ordered phases (shown as diamond-shaped and square symbols) at $x=\frac{1}{2}$. The zero of the energy corresponds to the pure constituent solids at their equilibrium lattice constant. The minimum of $\Delta E(a_{\mathrm{eq}})$ gives the alloys mixing enthalpy at $x=\frac{1}{2}$. (a) $Ag_{0.5}Pd_{0.5}$, (b) $Ag_{0.5}Au_{0.5}$. The negative sign of ΔH (alloy) implies that it is more stable than its disproportionation products. Note in (a) that the $L1_1$ ordered structure of AgPd is predicted to be more stable than the disordered alloy. The $B2$ structure is unstable with respect to phase separation [it has $\Delta H(B2) = +19.7$ meV/atom and therefore is outside the range of this figure]. Note in part (b) that the $L1_0$ ordered AgAu structure is more stable than the alloy.

where $\bar{a} = 4.032$ Å is the calculated linear average lattice parameter [Eq. (5)] of Ag and Au. This can be compared wit the experimental results

$$\Delta H(x=\tfrac{1}{2},\ T=800 \text{ K}) = -48.2 \text{ meV/atom (Ref. 66)}, \qquad a_{\mathrm{eq}} = 1.00\bar{a}_0 \text{ (Ref. 67)}, \tag{11}$$

where $\bar{a}_0$ is the linear average of the experimental lattice constants of Ag and Au. The calculated formation enthalpy for the ordered $L1_0$ structure (-60.5 meV/atom) is also negative and lower than that of the random alloy, hence, the $L1_0$ structure could be stable at low temperatures with respect to both phase separation and disordering. Again, the experimental phase diagram[70] does not extend to sufficiently low temperatures (it is limited to $T \gtrsim 1100$ K) to detect such a possible ordered phase. We have recently found[71] that other late-transition- (and noble-) metal alloys will also exhibit low-temperature ordering, despite the fact that d-band-filling argument[68] predict that they will phase separate.

B. Charge distributions

Self-consistent local-density calculations of the electronic structure of (ordered or disordered) compounds provide in a natural way the energy-minimizing electronic charge density $\rho(\mathbf{r})$. While this quantity is unique, attempts to characterize it in terms of *charge transfer between the subunits of the compound* (e.g., atomic spheres) are clearly arbitrary in that there is no unique or compelling way to apportion a three-dimensional solid into simple subunits. Correlating such charge transfer with the (thermochemically derived) Pauling electronegativity scale is hence problematic, precisely because of the arbitrariness in defining the subunits that exchange charge. Watson *et al.*[72] recently discussed the charge transfer in transition-metal alloys. They found that the tails of the charge density associated with the nearest neighbors to an atom can substantially change the charge count on the central atom. However, the charge-tail term itself is somehow arbitrary as is the charge on a site. Nevertheless, experiments and calculation give information about the actual distribution of charge in the solid and the "apparent" charge transfer is well defined. Here, we will use two different definitions of charge transfer in order to assess *qualitatively* the charge redistribution in an alloy. First, one can contrast the self-consistently calculated electronic density in the alloy

$$\rho_{\mathrm{alloy}}(\mathbf{r}) = \sum_{i}^{\varepsilon_F} N_i \psi_i(\mathbf{r}) \psi_i^*(\mathbf{r}) \tag{12}$$

(where the sum extends over all occupied states with weights N_i under the Fermi surface of energy ε_F) with that obtained by superposing overlapping ground-state spherical atomic charge densities

$$\rho_{\mathrm{sup}}(\mathbf{r}) = \sum_{\mathbf{R}_n} \sum_{\tau_\alpha} \rho_\alpha(\mathbf{r} - \mathbf{R}_n - \tau_\alpha) \tag{13}$$

[where $\rho_\alpha(|\mathbf{r}|)$ is the radial atomic charge density, $\mathbf{R}_n$ is the lattice vector, and τ_α is the atomic position vector in

the unit cell]. The differences

$$\Delta\rho_1(\mathbf{r}) \equiv \rho_{\text{alloy}}(\mathbf{r}) - \rho_{\text{sup}}(\mathbf{r}) \tag{14}$$

for AgPd and AgAu are depicted as contour plots in Fig. 6. We see that relative to this atomic reference system, charge is transferred *off* the atomic spheres (note the negative contours denoted as dashed lines in Fig. 6) *onto* the interstitial interatomic space. Hence, using Eq. (13) as a reference leads to the conclusion that *all* atoms lose charge from their atomic regions. Integration of $\Delta\rho_1(\mathbf{r})$ in the muffin-tin spheres about atomic sites indicates that Pd lost more charge than did Ag, in opposition to what might be concluded from elemental electronegativities (Table I). However, this is consistent with the fact that the configuration of Pd is d^{10} in the atom but d^9s^1 in the solid, and that the Pd s and d are more extended than the Ag s and d states (Table I). A similar situation exists in the AgAu alloy [Fig. 6(b)], where Au loses more charge than Ag. Note that crystallographically inequivalent atoms of the *same* chemical species have different charge transfer; for example, the $Ag^{(2)}$ site in AgAu [Fig. 6(b)], having only two Ag nearest neighbors, has more charge than the $Ag^{(8)}$ site that has eight like nearest neighbors.

A second definition of a reference system for assessment of charge transfer is the charge density of the elemental fcc solid of the same molar volume as the alloy. The relevant density fluctuation is then

$$\Delta\rho_2(\mathbf{r}) \equiv \rho_{\text{alloy}}(\mathbf{r}) - \rho_{\text{fcc}}(\mathbf{r}) \ . \tag{15}$$

Here, $\rho_{\text{fcc}}(\mathbf{r})$ is calculated in precisely an equivalent way as $\rho_{\text{alloy}}(\mathbf{r})$ (i.e., muffin-tin sphere radii, self-consistent conditions). Figure 7 depicts the dominant spherical part of $\Delta\rho_2(\mathbf{r})$ within the muffin-tin radii for AgPd and AgAu. We see that in the AgPd alloy [Fig. 7(a)] all Ag sites lose charge from their muffin-tin spheres in favor of the Pd spheres (in accord with what electronegativity suggests), whereas in the AgAu alloys [Fig. 7(b)] all Ag spheres *gain* charge with respect to the Au spheres (in opposition with the naive prediction based on electronegativity). Both directions of charge transfer are consistent, however, with the transfer of charge from the higher total electron density partner (Ag in Ag-Pd; Au in Ag-Au, see Fig. 2) to the partner with lower total electron density. Note further that chemically identical but crystallographically inequivalent sites again exhibit different degrees of charge transfer: in AgPd, the $Pd^{(2)}$-type atom (coordinated by ten Ag atoms) gains the most charge, whereas the $Pd^{(8)}$-type atom (coordinated only by four Ag atoms) gains the least charge. Similar comments (but with the reverse sign of charge transfer) apply to the $Ag^{(i)}$ sites in AgPd [Fig. 7(a)]. In AgAu [Fig. 7(b)], the $Ag^{(2)}$ ($Au^{(2)}$) sites gain (lose) the most charge, while $Ag^{(8)}$ ($Au^{(8)}$) gains (loses) the least charge. SCPA calculations do not exhibit any of these distinct charge "environmental effects" or their corresponding effects on the LDOS; instead, an average is produced. It is interesting to note that in AgAu most of the charge transfer occurs at the *boundary* of the atomic cell (and beyond), whereas in AgPd the charge transfer occurs mostly in the interior of the atomic cell (Fig. 7).

To further assess the type of charge transfer in the alloy, we have decomposed $\Delta\rho_2(\mathbf{r})$ of Eq. (15) into angular momenta components in the different atomic cells. Tables III and IV summarize the results for AgPd and

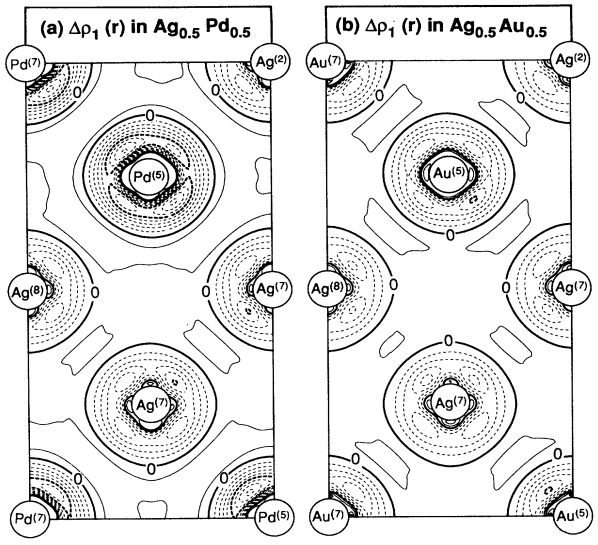

FIG. 6. Contour plots of the charge transfer $\Delta\rho_1(\mathbf{r})$ with respect to a superposition of spherical ground state atoms [Eq. (14)] for (a) AgPd and (b) AgAu in the (100) plane of the SQS-8. Solid contours, positive $\Delta\rho_1$; dashed contours, negative $\Delta\rho_1$. A contour step is $0.004e$/a.u. Note that charge is depleted from all atomic regions and deposited in the interstitial space. The lattice constant is $\bar{a}=3.928$ Å for AgPd and $\bar{a}=4.080$ Å for AgAu. Superscripts denote the number of like neighbors to each site.

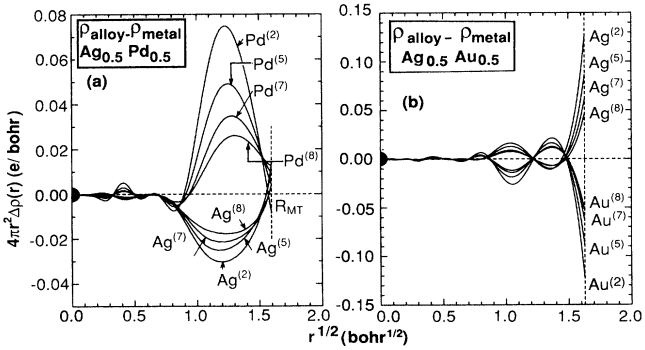

FIG. 7. Difference in total radial charge density $\Delta\rho_2(r)$ [Eq. (15)] between the alloy and the corresponding elemental fcc solid, both at the same lattice constant. (a) AgPd at $\bar{a}=3.928$ Å, (b) AgAu at $\bar{a}=4.080$ Å. To better resolve the function shown, we plot it vs $r^{1/2}$, not r. The vertical dashed line denotes the muffin-tin radii. The different curves correspond to the various (crystallographically inequivalent) sites; the superscripts on the atomic symbols denote the number of like first neighbors around each site. Note that the SCPA does not resolve this type of average charge fluctuation. In AgPd, Ag loses charge while in AgAu it gains charge. The amount of charge transfer is reduced as the number of like neighbors is increased.

TABLE III. Angular and atomic site decomposed charge (in unit of *e*) inside the muffin-tin (MT) sphere of radii of 2.55 a.u. for the $Ag_{0.5}Pd_{0.5}$ alloy in the SQS-8 structure and for its pure metal constituents at the alloy's volume. The alloy vs metal differences are also given. Charges outside the MT spheres are not included in this table. The column headed "first neighbor" gives the configurations of atoms in the first-neighbor shell (a total of 12 atoms), and "Degen." is the number of times that this type of atomic arrangement appears in the SQS-8 unit cell.

Atom	First neighbor	Degen.	$Q(s)$	$Q(p)$	$Q(d)$	$Q(f)$	Q(tot)
$Ag^{(2)}$	Ag_2Pd_{10}	1	0.455	0.373	9.128	0.045	10.015
$Ag^{(5)}$	Ag_5Pd_7	2	0.455	0.374	9.134	0.043	10.021
$Ag^{(7a)}$	Ag_7Pd_5	2	0.457	0.373	9.139	0.042	10.025
$Ag^{(7b)}$	Ag_7Pd_5	2	0.455	0.372	9.140	0.042	10.023
$Ag^{(8)}$	Ag_8Pd_4	1	0.455	0.373	9.143	0.041	10.027
Average	Ag_6Pd_6		0.456	0.373	9.137	0.043	10.023
Diff.			−0.010	−0.019	−0.007	+0.005	−0.031
Metal	$Ag_{12}Pd_0$		0.466	0.392	9.144	0.038	10.051
$Pd^{(2)}$	Pd_2Ag_{10}	1	0.383	0.302	8.357	0.039	9.094
$Pd^{(5)}$	Pd_5Ag_7	2	0.386	0.315	8.310	0.041	9.065
$Pd^{(7a)}$	Pd_7Ag_5	2	0.392	0.318	8.287	0.042	9.053
$Pd^{(7b)}$	Pd_7Ag_5	2	0.391	0.318	8.292	0.042	9.057
$Pd^{(8)}$	Pd_8Ag_4	1	0.390	0.323	8.281	0.043	9.052
Average	Pd_6Ag_6		0.389	0.316	8.302	0.042	9.062
Diff.			−0.011	−0.019	+0.086	−0.004	+0.050
Metal	$Pd_{12}Ag_0$		0.400	0.335	8.216	0.046	9.012

AgAu, respectively. They show the following.

(i) *s* charge transfer is decided primarily by the *s* chemical potential (ε_s in Table I). For example, in forming the AgAu alloy from the elemental solids, Ag loses *s* charge while Au gains *s* charge, consistent with the fact that Au has a lower *s* chemical potential [The small *s* charge transfer in AgPd does not follow this rule, partly because of sharp differences of the Fermi surface DOS of the two constituents in Fig. 3(b)].

(ii) Overall, relative to the elemental solids, Ag *gains* charge in the AgAu alloy, whereas Au loses charge as seen also in Fig. 7(b). In the AgPd alloy, the Ag site loses charge while the Pd site gains charge. Both trends are consistent with the picture of charge transfer from the fcc partner with higher total electron density to the one with lower total electron density (Fig. 2). This trend applies

TABLE IV. Angular and atomic site decomposed charge (in unit of *e*) inside the muffin-tin (MT) sphere of radii of 2.65 a.u. for the $Ag_{0.5}Au_{0.5}$ alloy in the SQS-8 structure and for its pure metal constituents at the alloy's volume. The alloy vs metal differences are also given. Charges outside the MT spheres are not included in this table. The column headed "First neighbor" gives the configurations of atoms in the first neighbor shell (a total of 12 atoms), and "Degen." is the number of times that this type of atomic arrangement appears in the SQS-8 unit cell.

Atom	First neighbor	Degen.	$Q(s)$	$Q(p)$	$Q(d)$	$Q(f)$	Q(tot)
$Ag^{(2)}$	Ag_2Au_{10}	1	0.442	0.393	9.277	0.044	10.172
$Ag^{(5)}$	Ag_5Au_7	2	0.450	0.385	9.271	0.040	10.160
$Ag^{(7a)}$	Ag_7Au_5	2	0.458	0.379	9.264	0.038	10.152
$Ag^{(7b)}$	Ag_7Au_5	2	0.458	0.379	9.267	0.038	10.155
$Ag^{(8)}$	Ag_8Au_4	1	0.460	0.375	9.263	0.037	10.148
Average	Ag_6Au_6		0.454	0.382	9.268	0.039	10.157
Diff.			−0.025	+0.017	+0.015	+0.008	+0.017
Metal	$Ag_{12}Au_0$		0.479	0.365	9.253	0.031	10.140
$Au^{(2)}$	Au_2Ag_{10}	1	0.640	0.385	8.837	0.037	9.912
$Au^{(5)}$	Au_5Ag_7	2	0.624	0.393	8.842	0.041	9.914
$Au^{(7a)}$	Au_7Ag_5	2	0.615	0.400	8.844	0.044	9.918
$Au^{(7b)}$	Au_7Ag_5	2	0.614	0.399	8.849	0.044	9.921
$Au^{(8)}$	Au_8Ag_4	1	0.610	0.400	8.847	0.045	9.918
Average	Au_6Ag_6		0.620	0.396	8.844	0.043	9.917
Diff.			+0.033	−0.024	−0.012	−0.008	−0.014
Metal	$Au_{12}Ag_0$		0.587	0.420	8.856	0.051	9.931

also to the d electron transfer.

(iii) The trends above are consistent with the qualitative analysis of observed Mössbauer isomer shift in AgAu alloys by Watson, Hudis, and Perlman[73] using a simple two-level model. Our calculation, however, produces smaller absolute magnitudes of the charge transfer than their (rather uncertain) estimates: Denoting by negative quantities loss of charge relative to the elemental solids, we find for the s charge transfer a $Ag^{-0.025}Au^{+0.033}$ configuration (Watson, Hudis, and Perlman[73] suggested $Ag^{-0.15}Au^{+0.13}$) and, for the d charge transfer, a $Ag^{+0.015}Au^{-0.012}$ configuration (Watson, Hudis, and Perlman[73] suggested $Ag^{+0.10}Au^{-0.08}$). Note that these results depend on the way space is divided. As recently discussed by Watson, Weinert, and Fernando[72] the charge-tailing effect plays a significant role in determining this s and d charge count.

(iv) As noted above, chemically independent but crystallographically inequivalent sites experience different magnitudes of charge transfer. Figure 8(a) plots for Ag-Au the total charge transfer of Table IV versus the number of like atoms in the first shell, showing a near-linear dependence. The same trend is seen for Ag-Pd and for Cu-Pd [Figs. 8(b) and 8(c), respectively], so these environmental effects are not accidental. Clearly, it will be unphysical to assign a constant charge to a given chemical species irrespective of its local environment. We can model the results of Fig. 8 by a simple linear form. Denoting by $\hat{S}_i$ the pseudospin operator for site i (-1 if occupied by A, $+1$ if occupied by B) and by $\hat{S}_k^{(i+1)}$ the spin on one of the 12 atoms that are nearest neighbors to i, Fig. 8 shows that the total charge transfer scales as

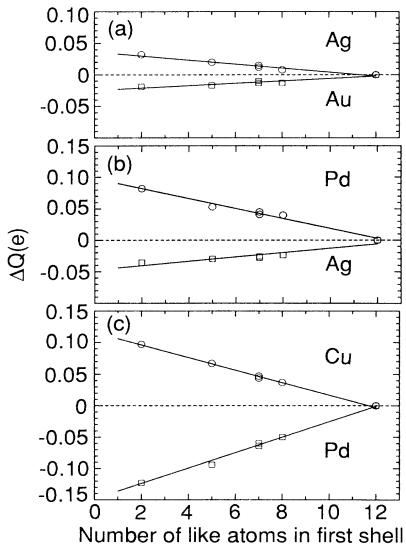

FIG. 8. Plot of the total charge transfer inside the muffin-tin spheres of Ag-Au, Ag-Pd, and Cu-Pd with respect to the pure solid (from Table IV) as a function of the number of like atoms in the first coordination shell. The linear dependence is modeled by Eq. (16). This general model has been used elsewhere (Ref. 8) to calculate lattice Madelung energies.

$$Q_i=\lambda \sum_{k=1}^{12} (\hat{S}_i-\hat{S}_k^{(i+1)}) , \tag{16}$$

with $\lambda\cong 2.6\times10^{-3}e$, $5.7\times10^{-3}e$, and $1.1\times10^{-2}e$ for Ag-Au, Ag-Pd, and Cu-Pd, respectively. This description of the dependence of charge transfer at fixed x on local coordination has been used previously[8] to model the electrostatic Madelung energies of random fcc lattice. It should be contrasted with the simplistic SCPA view that for fixed x Q_i is *independent* of the occupancy of the sites surrounding i, leading to a vanishing Madelung energy in the random alloy,[26(d)] hence to an overestimation of ordering energies.

C. Local density of states: General discussion of alloy effects

Before presenting our detailed DOS, we discuss the general factors affecting alloy DOS relative to those in the elemental solid constituents. There are four notable effects.[6,74–76]

(i) *Volume and sublattice deformation effects.*[74,76] The molar volume of alloys is usually intermediate between those of its constituents; when the latter have unequal volumes, the element with the smaller molar volume expands in the alloy medium while the one with the larger volume contracts. Compression displaces bonding states to deeper binding energies and broadens the d bands, whereas dilation has reverse effects. We expect such changes in the volume-mismatched AgPd system but not in the nearly volume-matched AgAu system (Table I). In addition, atoms can be displaced in an alloy off their nominal (e.g., fcc) lattice sites, causing additional (shear-type) deformation potential that can shift (and split degenerate) states.

(ii) Alloy fluctuation effects.[76] While in the pure fcc solid atoms are coordinated only by like species, in the alloys these neighboring atoms are partially replaced by unlike atoms. In general, there is a distribution of a variety of such local environments. If the two types of atoms have nonoverlapping bands, the altered local environment leads to an "off-resonance behavior," whereby the states of the central atom have in the alloy fewer matching states into which they can tunnel. This tends to break the broad DOS of the elemental solid into a series of narrower subbands, thus adding structure to the DOS. This structure and the attendant subband narrowing diminishes when the bands of the constituent solids overlap. Hence we expect to see some of this off-resonance behavior in the AgPd system (whose elemental bands are somewhat displaced with respect to one another, see Fig. 3), but not in the AgAu system exhibiting overlapping elemental bands (Fig. 4).

(iii) Band repulsion and hybridization effects. The alloy environment creates a perturbing potential $\delta V(\mathbf{r})$ that can be characterized as the difference between the actual alloy potential and that of a virtual crystal. $\delta V(\mathbf{r})$ has a structural component due to sublattice relaxation [item (i) above], as well as a chemical piece reflecting the potential change upon a constant-volume transmutation of a virtual atom into either A or B. The alloy perturbing po-

tential can couple VCA states either in a first-order manner (appropriate to degenerate VCA states) or in the second-order manner (non-degenerate VCA states). The coupling is inversely proportional to the initial energy difference between the states and leads to repulsion of the deep (shallow) state into yet deeper (shallower) binding energies. Furthermore, alloy band hybridization can induce LDOS, which does not exist in pure metal.

(iv) Charge-transfer effects. Band repulsion and hybridization effects can intermix states, resulting in charge transfer. Transfer of electronic charge onto (off) an atom raises (lowers) the Coulomb repulsion on that site, hence reducing (increasing) the binding energy of the level. The shift due to this effect can be modeled[6] through

$$\Delta_d^\alpha = U_{dd}^\alpha \Delta N_d^\alpha + U_{ds}^\alpha \Delta N_s^\alpha \ , \tag{17}$$

where U_{dd}^α and U_{ds}^α are the (positive) d-d and d-conduction Coulomb repulsion energies on site α, while ΔN_d^α and Δ_s^α are the excess d and conduction charges on site α, respectively, relative to the corresponding elemental solids. Note that the *direction* of d and conduction charge transfer need not be equal and hence, ΔN_d^α and ΔN_s^α could have opposite signs. The *intra*atomic Coulomb effect of Eq (17) might be partially offset by the *inter*atomic Madelung effect: transfer of charge off sublattice A and into sublattice B creates a repulsive Coulomb effect on B but also diminishes the Coulomb potential on this site due to the field created there by the oppositely charged sublattice A. Note, therefore, that this partial cancellation can lead to small changes in the DOS even if the total charge transfer is large. In what follows, we will use the above general analysis to discuss qualitatively our numerically obtained DOS.

D. Calculated local density of states

Figures 9 and 10 contrast the partial density of states of the AgPd and AgAu alloys, respectively, with those of pertinent elemental fcc solids. We have arbitrarily aligned the Fermi energies of each alloy with those of its constituent solids. The number shown in parentheses in each panel of Figs. 9 and 10 denote the angular momentum decomposed charge transfer within the muffin-tin sphere:

$$\Delta N_l^{A(B)} = \int_{-\infty}^{\varepsilon_F} D_l^{A(B)}(\varepsilon) d\varepsilon - \int_{-\infty}^{\varepsilon_F} d_l^{A(B)}(\varepsilon) d\varepsilon \ , \tag{18}$$

where $D_l^{A(B)}$ and $d_l^{A(B)}$ are the alloy and elemental solid DOS projected onto a given site (A or B) and angular momentum l. The two individual terms of Eq. (18) are given in Tables III and IV. Figure 11 depicts the total DOS of the alloys and the elemental constituents.

1. AgPd

The upper part of each panel in Fig. 9 depicts the site and angular momentum decomposed alloy LDOS inside the MT sphere, whereas the bottom part shows the corresponding decomposition in the pure elemental solids of equal molar volume. Comparison of the upper and lower panels shows the following: (i) The widths of the Ag and Pd d subbands in the alloy (e.g., measured arbitrarily but consistently at 20% of the maximum LDOS height) are modified relative to the corresponding values of the free elemental solids. In the $x=\frac{1}{2}$ alloy, the d band widths are 4.41 and 5.28 eV for Ag and Pd, respectively, while in the elemental solids they are 3.59 and 5.68 eV, respectively. (ii) The alloy Ag, d LDOS develops a tail in the low binding energy side [ε_F-2 eV in Fig. 9(c)] and a narrowing in the high binding energy side [ε_F-6 eV in Fig. 9(c)]. (iii) The alloy Pd, d LDOS shows just the reverse effect: the LDOS develops a tail at the deeper binding energy side relative to the pure metal and an enhancement in the low binding energy side. Figures 11(a)–11(c) further show that the rather sharp and pronounced features of the total (in the whole space, not MT spheres) DOS of elemental Ag and Pd are replaced in the alloy by a series of narrowly spaced peaks of lower intensity and larger width.

Considering the discussion of Sec. IV C, we note the following points.

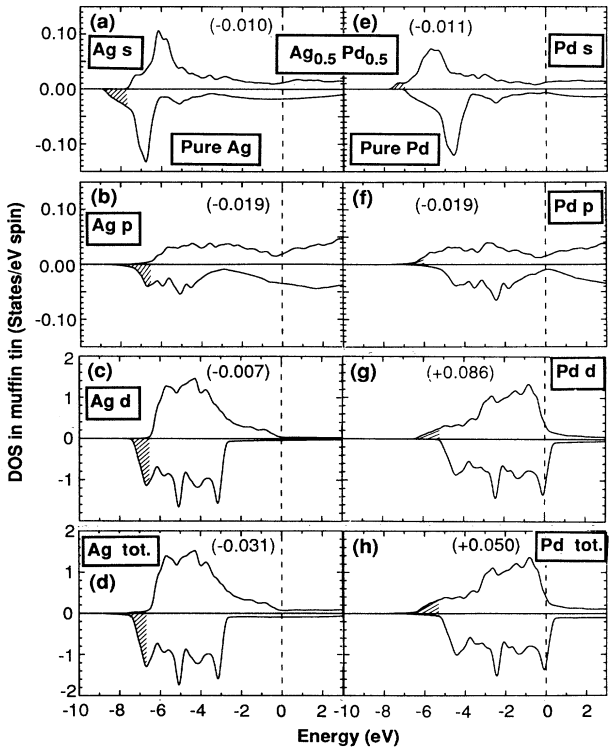

FIG. 9. Site and angular momentum decomposed LDOS inside the MT spheres for $Ag_{0.5}Pd_{0.5}$ (upper panels) and pure fcc solids (lower panels) at the same lattice constant. The alloy was modeled by averaging the results of SQS-8_a and SQS-8_b. Shaded areas highlight energy regions where significant changes occur. The Fermi energies of the alloy are aligned with those of the constituent solid. The number in parentheses gives the corresponding average charge transfer inside the MT spheres [defined in Eq. (18) and Tables III and IV] calculated at the alloy's volume. Negative (positive) values denote that the alloy atom lost (gained) electronic charge relative to the pure solid.

(i) Volume deformation effects (i.e., compression of Ag and dilation of Pd) shift the Ag state to deeper binding energies (and broaden their LDOS), while they shift the Pd states to shallower binding energies and narrow their LDOS (Fig. 3). These changes can be largely understood in terms of compression and dilation of the *elemental solids.* Indeed, compression of pure Ag from its equilibrium volume to that of the alloy [Eq. (8)] increases the d band width from 3.59 to 4.36 eV close to the partial width in the alloy (4.41 eV). Conversely, dilation of pure Pd to the alloy's volume reduces its bandwidth from 5.68 to 5.23 eV, again close to the alloy value (5.28 eV). Hence, alloy bandwidths remain virtually the same as in their elemental solids at *the same volume.* The fact that the Pd d band width in the alloy is slightly larger than in the (dilated) fcc metal is highlighted in Fig. 9(g) by the shaded area. This leads to a larger Pd d occupancy in the alloy, hence to additional Pd charge denoted in Fig. 9(g) as $\Delta Q = +0.086e$. Conversely, the narrowing of the Ag d band at deep energy in the alloy [Fig. 9(c)] leads to a (slight) *loss* of d charge ($\Delta Q = -0.007e$).

(ii) Alloy fluctuation effects smear the sharp features of the Ag and Pd DOS [Fig. 11(a) and 11(c)] into a series of narrowly spaced structures [Fig. 11(b)], reflecting the existence in the alloy of a *distribution* of local environments. To clarify environmental effects on the DOS, we show in Figs. 12(a) and 12(b) the Ag-centered [part (a)] and Pd-centered [part (b)] LDOS of $Ag_{0.5}Pd_{0.5}$. In the SCPA approach, there is but a single LDOS for each type, i.e., one for A and one for B. Figure 12 shows our

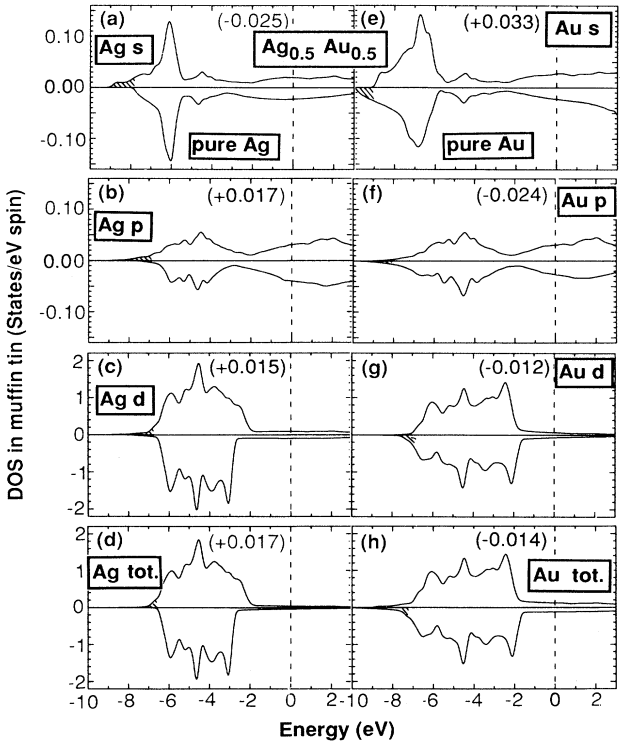

FIG. 10. Analogous to Fig. 9, but for $Ag_{0.5}Au_{0.5}$.

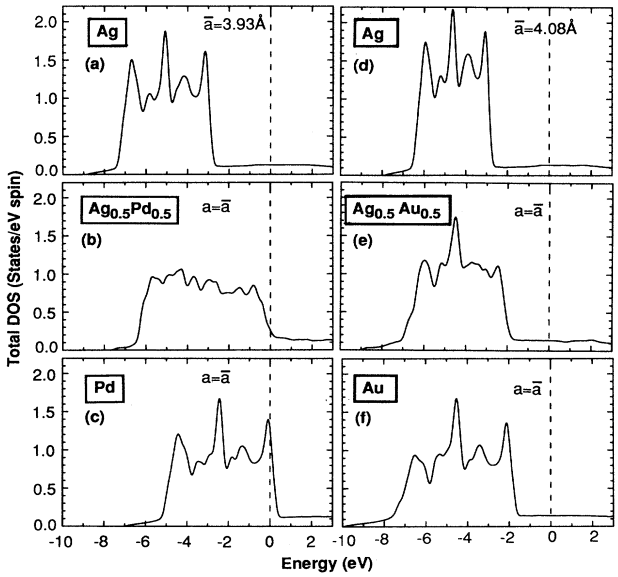

FIG. 11. Total DOS of (a) elemental solid Ag at $\bar{a} = 3.928$ Å, (b) the AgPd SQS at the same $\bar{a}$, and (c) elemental solid Pd at the same $\bar{a}$. The Fermi energies were aligned. Note that while Figs. 9(d) and 9(h) give the Ag and Pd DOS *inside* the MT spheres, the plots in parts (a) and (c) here give the full DOS in the whole lattice space. Part (d) gives the total DOS of elemental solid Ag at $\bar{a} = 4.080$ Å. Part (e) gives the results for the AgAu SQS at the same $\bar{a}$, while part (f) gives elemental solid Au at the same $\bar{a}$. Note that while Figs. 10(d) and 10(h) give the Ag and Pd DOS *inside* the MT spheres, the plots in parts (d) and (f) here give the full DOS in the whole lattice space.

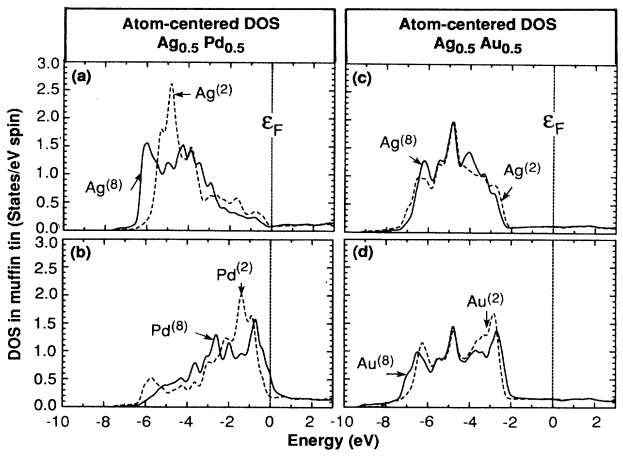

FIG. 12. This figure illustrates "environmental effects" on the DOS by showing atom-centered LDOS's. It gives the partial density of states inside the MT spheres for (a) $Ag^{(2)}$ and $Ag^{(8)}$ in $Ag_{0.5}Pd_{0.5}$, (b) $Pd^{(2)}$ and $Pd^{(8)}$ in $Ag_{0.5}Pd_{0.5}$, (c) $Ag^{(2)}$ and $Ag^{(8)}$ in $Ag_{0.5}Au_{0.5}$, and (d) $Au^{(2)}$ and $Au^{(8)}$ in $Ag_{0.5}Au_{0.5}$. The superscripts denote the number of line atoms in the nearest-neighbor shell. Note in (a) that Ag coordinated locally by only two Ag atoms has a narrower DOS than Ag coordinated by eight Ag atoms. These effects are weaker in the common band AgAu system.

results for *two* representative Ag and two Pd atoms in the alloy: one coordinated just by two like atoms [$A^{(2)}$] and one coordinated by eight like atoms [$A^{(8)}$]. We have seen in Fig. 7 that local coordination sensitively affects the charge distribution about a site. Figures 12(a) and 12(b) show that it also affects the DOS. Notice that the Ag bandwidth depends strongly on its nearest-neighbor environment (e.g., the bandwidth of $Ag^{(8)}$ is much larger than that of $Ag^{(2)}$). This is consistent with the fact that $Ag^{(8)}$ has more charge than $Ag^{(2)}$ [Fig. 7(a)]. We expect that much of this structure would be absent in effective-medium theories that consider but a single, effective environment. Similar effects were noticed by Gonis, Butler, and Stocks[10] in their embedded cluster approach; the present SQS approach provides a natural way for assembling such atom-centered DOS's (Fig. 12) into total DOS (Fig. 11).

(iii) Band repulsion and hybridization effects are significant for the AgPd DOS. For Ag, since it has lower energy, the level repulsion enhances the deeper binding energy portion of its LDOS while hybridization with Pd states (which have lower binding energy) creates a tail in the lower binding energy portion of its DOS. Opposite effects exist for Pd [Fig. 9(g)].

2. *Ag Au*

Figure 10 (LDOS) and Figs. 11(d)–11(f) (total DOS) show the following features. (i) The Ag *d* band broadens in the alloy relative to the same band in pure Ag [4.23 eV vs 3.59 eV, measured arbitrarily at 20% of the maximum height in Fig. 10(c)], while the Au *d* band is narrower in the alloy (4.88 eV) than in the pure Au (5.28 eV). (ii) The Ag *s* and *p* LDOS develops a high-binding energy structure [Figs. 10(a) and 10(b)], whereas the Au *s* and *p* LDOS are reduced in the high-binding energy regions [Figs. 10(e) and 10(f)]. (iii) The total DOS [Fig. 11(e)] shows a simple "common band" behavior whose structure resembles that of the constituents [Figs. 11(d) and 11(f)].

Considering the discussion of Sec. IV C, we note the following. (i) There are no volume deformation effects in this lattice-matched system. (ii) Alloy fluctuation effects are smaller [Figs. 12(c) and 12(d)] compared with those in the AgPd alloy since the bands of the Ag and Au are fully overlapping (Fig. 4). (iii) The broadening (narrowing) of Ag (Au) in the alloy evident in Figs. 10(c) and 10(g) is caused by the hybridization of the center atom with its nearest-neighbor environment. This is consistent with the fact that Au has loosely bonded electrons and hence larger bandwidth while Ag has more tightly bonded electrons and hence smaller bandwidth. (iii) The loss of Ag *s* charge leads to a shift of its *s*-like LDOS to deeper binding energies [Fig. 10(a)] whereas the gain of Au *s* charge displaces the *s*-like DOS to smaller binding energies [Fig. 10(e)]. (iv) In AgAu, the Ag atom *gains d* charge [Fig. 10(c)], while in AgPd, the Ag atom *loses d* charge [Fig. 9(c)]. Concomitantly, the Ag *d* band in AgAu broadens at deep binding energies relative to fcc Ag, while the Ag *d* band in AgPd narrows in the deep binding energy regime.

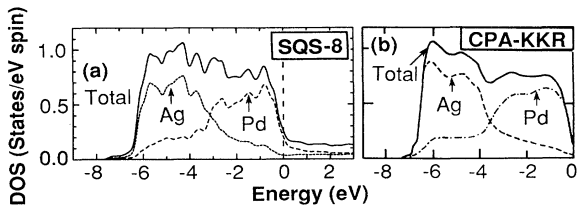

FIG. 13. (a) Comparison of the total DOS (in the whole space) of $Ag_{0.5}Pd_{0.5}$ as obtained by averaging the SQS-8_a and SQS-8_b results, with the decomposition into Ag and Pd contributions (in the alloy, not pure solids) in MT spheres. (b) Results of the CPA-KKR for $Ag_{0.5}Pd_{0.5}$ (Refs. 1 and 44). Note that the distinct structure found here in the total DOS [solid line in part (a)] is absent in the effective-medium results [solid line in part (b)].

E. Total density of states

Figures 13 and 14 show the total DOS of AgPd and AgAu (solid lines), along with their decompostion into the constituents. In the case of AgPd, where previous CPA calculations are available,[1,21(c),43-45] we show a comparison of our results with those of Winter and Stocks[43] [Fig. 13(b)]. As discussed above, the SQS exhibits a distribution of various local environments leading to a substantial structure in the DOS [solid line in Fig. 13(a)] that is missing in the CPA model [solid line in Fig. 13(b)]. The overall width of the DOS and its decomposition into Ag and Pd components are similar in both calculations. (A similar SCPA calculation[46] for AgAu at $x=\frac{1}{2}$ is, however, lacking).

V. CONCLUSIONS

We have seen that a *structural theory* of alloys considers the existence of a distribution of chemically distinct local environments whose average gives the correct macroscopic composition. *Nonstructural, effective-medium*

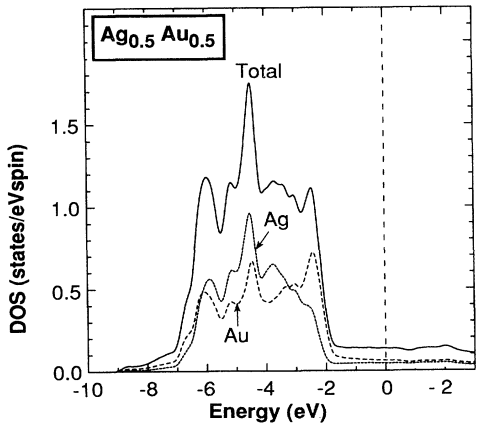

FIG. 14. Comparison of the total DOS of $Ag_{0.5}Au_{0.5}$ as obtained by averaging its SQS-8_a and SQS-8_b results (solid line) with the decomposition into Ag and Au contributions (in the alloy, not pure solids) in the MT spheres.

theories describe, on the other hand, all local environments as being identical, so *each* is characterized by the macroscopic composition. They are indeed intended to determine only the statistically average LDOS of the component species, producing a single function that does not resolve environmental effects. While there certainly exist alloy properties that depend only on the global composition (e.g., the molecular weight of $A_{1-x}B_x$), many properties reflect local coupling and hence depend specifically on the atomic arrangements and composition about sites. In applications where a single averaged DOS suffices, the SCPA is adequate. If, on the other hand, one is interested in local environmental effects, one needs to go beyond the SCPA. We know, for example, that one component of the total energy of an alloy—the electrostatic point charge energy—is incorrectly described by such effective medium single site approaches that neglect fluctuations.[8] Since there are no parallel CPA and SQS calculations of the total energy, it is still not clear whether the nonelectrostatic terms in the total CPA energy can compensate for the error made in the electrostatic part. We must await such comparisons. We have seen that a structural theory of AgPd and AgAu alloy leads to a significant environmental effect on the charge densities around nominally chemically identical atoms (Figs. 6–8), as well as to environmental effects on the density of states (Fig. 12). We find that, owing to the significant separation of the *d* bands of the constituents in AgPd, environmental effects are rather pronounced in its DOS [Figs. 12(a) and 12(b)]. On the other hand, owing to the small *d* band separation but significant *s* orbital energy difference in AgAu, environmental effects are more pronounced for the charge transfer [Figs. 6(b) and 7(b)] but less pronounced for the DOS [Figs. 12(c) and 12(d)]. We expect that transition metal alloys whose constituents differ significantly both in electronegativity and in *d* band energies would exhibit the largest environmental effects in charge fluctuations as well as DOS. This has been recently confirmed in our SQS calculation for the DOS of $Cu_{0.75}Pd_{0.25}$.[77] Owing to the large size mismatch between the constituents ($\sim 7.5\%$) we find significant relaxation effects (the Pd—Pd bond length is longer than the VCA average value). These, in turn, shift the Pd LDOS by ~ 1 eV to lower binding energies.

The SQS model is readily applicable to metals as well as to semiconductor[16,30,31] alloys, permits the effective use of full-potential self-consistent electronic structure methods, and predicts ground-state cohesive properties (mixing enthalpies, equilibrium lattice constants) as well as single-particle DOS. The method can be improved systematically by using larger sizes in constructing the SQS. The results could be compared to future extensions of the SCPA to include inhomogeneous effects.

ACKNOWLEDGMENTS

This work was supported by the Office of Energy Research (OER) [Division of Materials Science of the Office of Basic Energy Science (BES)], U.S. Department of Energy, under Contract No. DE-AC02-77-CH00178. We are grateful for an OER-BES grant of computer time, which made this work possible.

[1]G. M. Stocks and H. Winter, in *The Electronic Structure of Complex Systems,* edited by P. Phariseau and W. M. Temmerman (Plenum, New York, 1984), p. 463.

[2]D. A. Papaconstantopoulos, in *Alloy Phase Stability,* edited by G. M. Stocks and A. Gonis (Kluwer Academic, Dordrecht, 1989), p. 351.

[3]F. Ducastelle, in *Alloy Phase Stability* (Ref. 2), p. 293.

[4]L. Nordheim, Ann. Phys. (Leipzig) **9**, 607 (1931).

[5]P. Soven, Phys. Rev. **178**, 1136 (1969); B. Velický, S Kirkpatrick, and H. Ehrenreich, *ibid.* **175**, 747 (1968).

[6]C. D. Gelatt, Jr. and H. Ehrenreich, Phys. Rev. B **10**, 398 (1974).

[7]M. Sluiter and P. E. A. Turchi, Phys. Rev. B **40**, 11 215 (1989).

[8]R. Magri, S.-H. Wei, and A. Zunger, Phys. Rev. B **42**, 11 388 (1990).

[9]Z. W. Lu, S.-H. Wei, A. Zunger, S. Frota-Pessoa, and L. G. Ferreira, Phys. Rev. B **44**, 512 (1991).

[10]A. Gonis, W. H. Butler, and G. M. Stocks, Phys. Rev. Lett. **50**, 1482 (1983).

[11]J. Van der Rest, F. Gautier, and F. Brouers, J. Phys. F **5**, 2283 (1975).

[12]M. Cyrot and F. Cryot-Lackmann, J. Phys. F **6**, 2257 (1976).

[13]L. C. Davis, Phys. Rev. B **28**, 6961 (1983).

[14]L. C. Davis and H. Holloway, Solid State Commun. **64**, 121 (1987).

[15]R. Alben, M. Blume, H. Krakauer, and L. Schwartz, Phys. Rev. B **12**, 4090 (1975); J. J. Rehr and R. Alben, *ibid.* **16**, 2400 (1977); R. Alben, M. Blume, and M. McKewon, *ibid.* **16**, 3829 (1977).

[16]K. C. Hass, L. C. Davis, and A. Zunger, Phys. Rev. B **42**, 3757 (1990).

[17](a) J. C. Mikkelsen and J. B. Boyce, Phys. Rev. Lett. **49**, 1412 (1982); Phys. Rev. B **28**, 7130 (1983); J. B. Boyce and J. C. Mikkelsen, *ibid.* **31**, 6903 (1985); (b) J. B. Boyce and J. C. Mikkelsen, in *Ternary and Multinary Compounds,* edited by S. K. Deb and A. Zunger, (Materials Research Society, Pittsburgh, 1987), p. 359.

[18]A. Balzarotti, N. Motta, M. Czyzyk, A. Kisiel, M. Podgorny, and M. Zimnal-Starnawska, Phys. Rev. B **30**, 2295 (1984); A. Balzarotti, Physica **146B**, 150 (1987); A. Balzarotti, N. Motta, A. Kisiel, M. Zimnal-Starnawska, M. T. Czyzyk, and M. Podgorny, Phys. Rev. B **31**, 7526 (1985); P. Letardi, N. Motta, and A. Balzarotti, J. Phys. C **20**, 2583 (1987).

[19]B. A. Bunker, J. Vac. Sci. Technol. **5A**, 3003 (1987); Q. T. Islam and B. A. Bunker, Phys. Rev. Lett. **59**, 2701 (1987).

[20]P. Weightman, H. Wright, S. D. Waddington, D. van der Marel, G. A. Sawatzky, G. P. Diakun, and D. Norman, Phys. Rev. B **36**, 9098 (1987) showed by EXAFS measurements that 1 at.% Pd in Cu changes the Cu-Pd nearest-neighbor distance to 2.560 Å, away from the 2.515-Å Cu—Cu bond distance in pure Cu. See also Ch. Barrett and T. B. Massalski, *Structure of Metals* (Pergamon, Oxford, 1980), p. 370; G. Renaud, N. Motta, F. Lancon, and M. Belakhovsky, Phys. Rev. B **38**, 5944 (1988) have shown in EXAFS measurements on $Ni_{1-x}Au_x$ that there are distinct Ni—Ni, Ni—Au, and Au—Au bond lengths.

[21]The consequences of atomic relation in metal alloys on the electronic structure was discussed, e.g., for CuPd by (a) J.

Mašek and J. Kudrnovský, Solid State Commun. **58**, 67 (1986); (b) J. Kudrnovský and V. Drchal, *ibid.* **70**, 67 (1989); (c) J. Kudrnovský and V. Drchal, Phys. Rev. B **41**, 7515 (1990).

[22]F. Ducastelle, J. Phys. C **7**, 1795 (1974); K. C. Hass, R. J. Lempert, and H. Ehrenreich, Phys. Rev. Lett. **52**, 77 (1984); R. J. Lempert, K. C. Hass, and H. Ehrenreich, Phys. Rev. B **36**, 1111 (1987).

[23]R. Mills and P. Ratanavararaka, Phys. Rev. B **18**, 5291 (1978).

[24]T. Kaplan, P. L. Leath, L. J. Gray, H. W. Diehl, Phys. Rev. B **21**, 4230 (1980).

[25]A. Zin and E. A. Stern, Phys. Rev. B **31**, 4954 (1985); E. A. Stern and A. Zin, *ibid.* **9**, 1170 (1974).

[26](a) D. D. Johnson, D. M. Nicholson, F. J. Pinski, B. L. Györffy, and G. M. Stocks, Phys. Rev. Lett. **56**, 2088 (1986); (b) Phys. Rev. B **41**, 9701 (1990); (c) J. B. Staunton, D. D. Johnson, and F. J. Pinski, Phys. Rev. Lett. **65**, 1259 (1990); (d) D. D. Johnson, P. E. A. Turchi, M. Sluiter, D. M. Nicholson, F. J. Pinski, and G.M. Stocks, in *Alloy Phase Stability and Design,* Materials Research Society Symposium 186, edited by G. M. Stocks, D. P. Pope, and A. F. Giamer (Materials Research Society, Pittsburgh, 1991) , Vol. 21.

[27]*Local Density Approximation in Quantum Chemistry and Solid State Physics,* edited by J. P. Dahl and J. Avery (Plenum, New York, 1984).

[28]*The Electronic Structure of Complex Systems,* Vol. 113 of *NATO Advanced Study Institute, Series B: Physics,* edited by P. Phariseau and W. M. Temmerman (Plenum, New York, 1982).

[29]*Electronic Structure, Dynamics, and Quantum Properties of Condensed Matter,* Vol. 121 of *NATO Advanced Study Institute, Series B: Physics,* edited by J. T. Deveese and D. Van Camp (Plenum, New York, 1984).

[30]A. Zunger, S. H. Wei, L. G. Ferreira, and J. E. Bernard, Phys. Rev. Lett. **65**, 353 (1990).

[31](a) S.-H. Wei, L. G. Ferreira, J. E. Bernard, and A. Zunger, Phys. Rev. B **42**, 9622 (1990); (b) S.-H. Wei and A. Zunger, *ibid.* **43**, 1662 (1991).

[32]J. M. Sanchez, F. Ducastelle, and D. Gratias, Physica A **128**, 334 (1984).

[33]P. Hohenberg and W. Kohn, Phys. Rev. **136**, B864 (1964).

[34]W. Kohn and L. J. Sham, Phys. Rev. **140**, A1133 (1965).

[35]S.-H. Wei and H. Krakauer, Phys. Rev. Lett. **55**, 1200 (1985) and references therein.

[36]J. E. Bernard and A. Zunger, Phys. Rev. B **44**, 1663 (1991).

[37]B. L. Gyorffy, A. Pindor, and W. M. Temmerman, Phys. Rev. Lett. **43**, 1343 (1979).

[38]B. L. Gyorffy and G. M. Stocks, J. Phys. F **10**, L321 (1980).

[39]A. J. Pindor, W. M. Temmerman, B. L. Gyorffy, and G. M. Stocks, J. Phys. F **10**, 2617 (1980).

[40]G. M. Stocks and W. H. Butler, in *Physics of Transition Metals,* edited by P. Rhodes (Institute of Physics and Physical Society, London, 1981).

[41]P. J. Durham, N. K. Allen, B. L. Gyorffy, J. B. Pendry, and W. M. Temmerman, in *Physics of Transition Metals,* edited by P. Rhodes (Institute of Physics and Physical Society, London, 1981).

[42]G. M. Stocks and W. H. Butler, Phys. Rev. Lett. **48**, 55 (1982).

[43]H. Winter and G. M. Stocks, Phys. Rev. B **27**, 898 (1983).

[44]J. Kudrnovský and J. Mašek, Phys. Rev. B **31**, 6424 (1985).

[45]P. M. Laufer and D. A. Papaconstantopoulos, Phys. Rev. B **35**, 9019 (1987).

[46]H. Ebert, P. Weinberger, and J. Voitländer, Z. Phys. B **63**, 299 (1986).

[47]L. Pauling, *The Nature of the Chemical Bond,* 3rd ed. (Cornell University Press, New York, 1960), p. 93.

[48]D. E. Eastman, Phys. Rev. Lett. **2**, 1 (1970).

[49]R. W. G. Wyckoff, *Crystal Structures,* 2nd ed. (Interscience, New York, 1963), Vol. 1, p. 10.

[50]D. M. Ceperley and B. J. Alder, Phys. Rev. Lett. **45**, 566 (1980).

[51]J. P. Perdew and A. Zunger, Phys. Rev. B **23**, 5048 (1981).

[52]*International Tables for Crystallography,* edited by T. Hahn (Reidel, Dordrecht, 1983), p. 150.

[53]H. J. Monkhorst and J. D. Pack, Phys. Rev. B **13**, 5188 (1976).

[54]G. Lehman and M. Taut, Phys. Status Solidi **54**, 469 (1971).

[55]A. H. MacDonald, J. M. Daams, S. H. Vosko, and D. D. Koelling, Phys. Rev. B **23**, 6377 (1981).

[56]A. H. MacDonand, J. M. Daams, S. H. Vosko, and D. D. Koelling, Phys. Rev. B **25**, 713 (1982).

[57]L. Hedin and B. I. Lundqvist, J. Phys. C **4**, 2063 (1971).

[58]N. E. Christensen, Phys. Status Solidi B **54**, 551 (1972).

[59]T. Loucks, *Augmented Plane Wave Method* (Benjamin, New York, 1967).

[60]J. C. Slater, Phys. Rev. **51**, 846 (1937).

[61]N. E. Christensen and B. O. Seraphin, Phys. Rev. B **4**, 3321 (1971); N. E. Christensen, *ibid.* **13**, 2698 (1976).

[62]F. J. Himplsel and D. E. Eastman, Phys. Rev. B **18**, 5236 (1978).

[63]P. S. Wehner, R. S. Williams, S. D. Kevan, D. Denley, and D. A. Shirley, Phys. Rev. B **19**, 6164 (1980).

[64]K. A. Mills, R. F. Davis, D. Kevan, G. Thornton, and D. A. Shirley, Phys. Rev. B **22**, 581 (1980).

[65]N. Takeuchi, C. T. Chan, and K. M. Ho, Phys. Rev. **40**, 1565 (1989).

[66]*Selected Values of the Thermodynamic Properties of Binary Alloys,* edited by R. Hultgren, P. D. Desai, D. T. Hawkins, M. Gleiser, and K. K. Kelley (American Socieity for Metals, Metals Park, Ohio, 1973).

[67]*Numerical Data and Functional Relationships in Science and Technology,* edited by K.-H. Hellwege and A. M. Hellwege, Londolt-Börnstein, New Series, Group III, Vol. 6 (Springer-Verlag, Berlin, 1971).

[68]A. Bieber and F. Gautier, Acta. Metall. **34**, 2291 (1986); *ibid.* **35**, 1839 (1987).

[69]S. Takizawa and K. Terakura, Phys. Rev. B **39**, 5792 (1989).

[70]*Binary Alloy Phase Diagrams,* edited by J. L. Murray, L. H. Bennett, and H. Baker (American Society of Metals, Metals Park, Ohio, 1986), Vol. 1, pp. 5 and 55.

[71]Z. W. Lu, S.-H. Wei, and A. Zunger, Phys. Rev. Lett. **66**, 1753 (1991).

[72]R. E. Watson, M. Weinert and G. M. Fernando, Phys. Rev. B **43**, 1446 (1991).

[73]R. E. Watson, J. Hudis, and M. L. Perlman, Phys. Rev. B **4**, 4130 (1971).

[74]C. D. Gelatt, H. Ehrenreich, and R. E. Watson, Phys. Rev. B **15**, 1613 (1977).

[75]L. Hodges, R. E. Watson, and H. Ehrenreich, Phys. Rev. B **5**, 3953 (1972).

[76]V. L. Moruzzi, A. R. Williams, and J. F. Janak, Phys. Rev. B **10**, 4856 (1974).

[77]Z. W. Lu, S.-H. Wei, and A. Zunger, Phys. Rev. B **44**, 3387 (1991).